Materials and Design 132 (2017) 375–384

Contents lists available at ScienceDirect

Materials and Design

journal homepage: www.elsevier.com/locate/matdes

Pattern transformation of single-material and composite periodic cellular structures

Yuhao He [a,b], Yu Zhou [a], Zishun Liu [a,*], K.M. Liew [b,*]

[a] International Center for Applied Mechanics, State Key Laboratory for Strength and Vibration of Mechanical Structures, Xi'an Jiaotong University, Xi'an 710049, China
[b] Department of Architecture and Civil Engineering, City University of Hong Kong, Tat Chee Avenue, Kowloon, Hong Kong, China

HIGHLIGHTS

- Novel composite periodic cellular metamaterials with soft matrix and interfacial layers are designed.
- The composite periodic cellular structures are successfully fabricated via different experimental methods.
- The buckling modes phase diagram of the composite periodic cellular structures is obtained.
- A method to predict the critical strains of the single-material and composite periodic cellular structures is proposed.

GRAPHICAL ABSTRACT

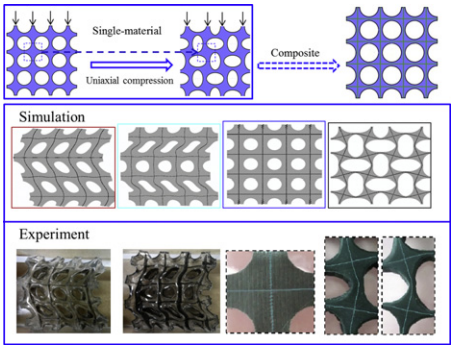

ARTICLE INFO

Article history:
Received 29 May 2017
Received in revised form 10 July 2017
Accepted 11 July 2017
Available online 12 July 2017

Keywords:
Buckling
Composite
Metamaterial
Periodic cellular structure
Interfacial layer

ABSTRACT

Novel pattern transformation occurs when periodic cellular structures are compressed beyond a critical value. We have designed a kind of composite periodic cellular metamaterials with soft matrix and interfacial layers, and the buckling modes phase diagram of the composites is obtained. The buckling behaviors of the composites are studied both in numerical simulations and experiments. It is evident that the critical strains of composite periodic cellular structures are always lower than those of single-material periodic cellular structures, regardless of the interfacial layer is stiffer or softer than the matrix materials. We have proposed a theoretical method to predict the critical strain for the pattern transformation of single-material periodic cellular structures. Furthermore, based on the simulation and experiment results, the theoretical method is developed to predict the critical strain for a definite range of combinations of materials and porosities of the periodic cellular composites.

1. Introduction

Metamaterials are rationally engineered multiscale materials whose equivalent physical properties are governed by their architectures rather than compositions. Because of their capability of exhibiting novel properties for broad ranges of potential applications, metamaterials have attracted great interests in recent years [1,2]. When metamaterials are artificially and properly designed, the metamaterials can exhibit negative refractive index [3–6], or negative Poisson's ratio [7–12], or acoustic cloaking [13,14], which are impossible to exist in conventional materials. Among them, the auxetic (negative Poisson's ratio) response to an external load is perhaps the most well-known and of particular interests [15].

Materials with auxetic behavior will contract (expand) transversally when they are axially compressed (stretched). The auxetic behavior has

* Corresponding authors.
E-mail addresses: zishunliu@mail.xjtu.edu.cn (Z. Liu), kmliew@cityu.edu.hk (K.M. Liew).

http://dx.doi.org/10.1016/j.matdes.2017.07.022
0264-1275/

been observed in a variety of systems, such as layered ceramics [16], re-entrant foams [17], textile structures [18], origami [19] and kirigami [20, 21] geometries, structures with rotating elements [22–24], corrugated sheets [25] and other artificially designed structures [26–29]. Periodic cellular structures and periodic lattice structures are two common types of the metamaterials which have auxetic behavior.

The inspiration for periodic cellular structures comes from natural world, such as iridescent phenomena in butterflies, beetles, moths, birds and fish. When this kind of periodic cellular structures is compressed beyond a critical value, a novel pattern transformation will appear. The pattern transformation of periodic cellular structures is caused by local elastic instabilities and often reversible and repeatable [30]. Along with the local buckling, the periodic cellular structure will undergo a transformation from initial circular voids to alternating mutually orthogonal elliptic holes. There are many factors that affect the pattern transformation, such as the initial porosity of structures [8], the arrangement of holes [31], the loading condition [32,33], the shape [34] and inclusions [35] of holes, and the viscoelastic property of component materials [36].

Periodic lattice structures are advanced light weight periodic materials with specific high strength and stiffness [37,38], and have the potential application in aerospace engineering [39], energy absorption, and as the core of lightweight sandwich panels [40]. Buckling of columns is the dominated collapse mode of periodic lattice structures. But the local buckling induced pattern transformation may not be a preferred buckling mode, for example, the stress of local buckling for a square honeycomb lattice is always higher than the stress that trigger the global buckling mode [41–43]. In general, pattern transformation is a buckling mode that will surely appear in lattice structures.

However, most of the previous studies on the buckling of periodic cellular structures were in numerical simulations or experiments [44–49]. Only a few theoretical studies are available, and most of the theoretical studies are focused on lattice structures [41,50,51] based on the beam-column solution as presented by Timoshenko and Gere [52], or through analogy with rigid link lattice systems [27], or based on an energy approach [24]. Though a beam model was recently developed by Heitkam et al. [53] to study the elastic properties of cellular materials with spherical voids, the model is for a general porous material and does not consider the buckling properties. It still lacks of a theoretical approach to predict the pattern transformation behavior for periodic cellular structures.

To fill this apparent gap, here we proposed a theoretical method to predict the critical strain for the pattern transformation of periodic cellular structures. Since the weakest section dominates the pattern transformation, the periodic cellular structures with circular holes can be simplified as a cross-shaped structure (a structure with square holes) with the weakest section, and can be dealt with via the buckling theory of square lattice frames. However, in our study, we have found an interesting phenomenon that, just by introducing very thin interfacial layers into the single-material periodic cellular structure, the critical strain for pattern transformation can be significantly reduced. At the same time, the buckling behaviors of composite periodic cellular structures with soft matrix and interfacial layers are more variety. This is because wrinkling of the interfacial layers is influenced by many factors, which has been reported by Li et al. [54] in the work of "Wrinkling of interfacial layers in stratified composites". To cover the most possibilities for the various buckling behaviors of periodic cellular composites, we have performed a number of finite element simulations and experimental studies with different material combinations and porosities, and drawn a phase diagram of the various buckling modes based on these results. Furthermore, we presented an analytical method to predict the critical strain for a definite range of combinations of materials and porosities of the composite periodic cellular structures based on the simulation and experiment results.

2. Materials and methods

Pattern transformation is a novel property of periodic cellular structure, and it appears when the periodic cellular structure is compressed beyond a critical value [30], as shown in Fig. 1. The pattern transformation of periodic cellular structures is induced by local elastic instabilities and often reversible and repeatable. The nominal strain corresponding to the pattern transformation is named critical strain in this study.

2.1. Finite element simulation

2.1.1. Model and material properties

The pattern transformation of periodic cellular structures has been studied for many years. The periodic cellular structure is composed of primitive cells as shown in the left of Fig. 1, and at least 2×2 primitive cells should be employed to characterize the pattern transformation because the periodicity is $p = (2,2)$ [55]. However, the global buckling of periodic cellular structure has no periodic cell and the buckling shapes vary as the sizes of the models change. Considering the difference between pattern transformation and global buckling, the size of representative volume element (RVE) model for a periodic cellular structure is taken as 2×2 and 4×4 primitive cells, with circular holes of radius ranging from $r = 3.2$ mm to 4.9 mm and a nearest center-to-center spacing of $l = 10$ mm, which give porosities from about $\phi = 0.322$ to 0.754. The schematic for pattern transformation of RVE model consist of 4×4 primitive cells is shown in Fig. 1. The material properties are taken as $E = 3$ MPa and $\nu = 0.4995$.

Based on the study of pattern transformation in periodic cellular structures, we designed a kind of composite periodic cellular structures with interfacial layers, and the primitive cell is shown in Fig. 2(b). The size of the RVE model for a composite periodic cellular structure consists of 4×4 primitive cells is shown in Fig. 2(a), with a nearest center-to-center spacing $l = 10$ mm and different radii r of circular holes ranging from $r = 2.4$ mm to 4.9 mm, which gives the porosities from 0.181 to 0.754. As we can imagine, it will play a bigger role to the buckling of composites as the interfacial layer is getting thicker. In this study, we take the thickness of interfacial layers to be $t = 0.05$ mm for the cases with a center-to-center spacing $l = 10$ mm as an example, which gives a thickness-to-length ratio of $t/l = 0.005$ between the thickness of the interfacial layers and center-to-center spacing. Though the interfacial layers are very thin compared to the cellular composite, the interfacial layers can significantly influence the buckling behavior of periodic cellular structures.

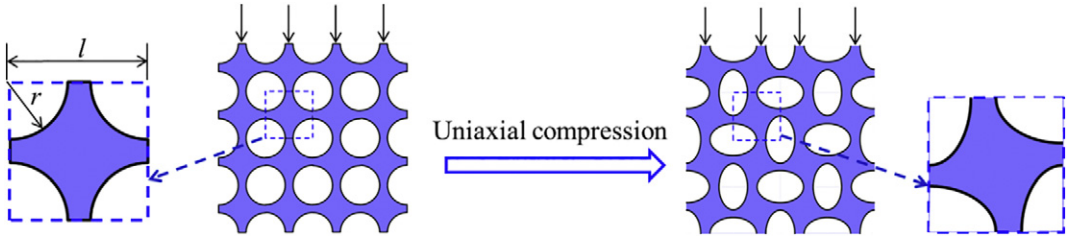

Fig. 1. Schematic of pattern transformation for periodic cellular structures.

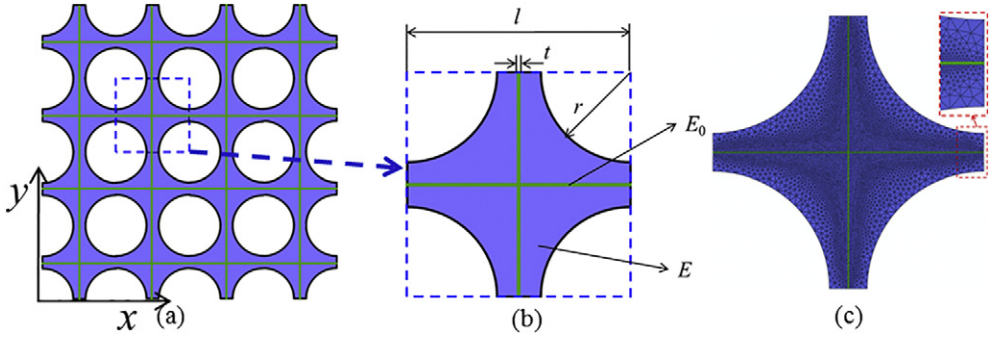

Fig. 2. (a) Schematic of composite periodic cellular structures with interfacial layers. (b) Geometry and material details of the composite periodic cellular structures in a minimum unit cell. (c) Mesh details of the composite periodic cellular structures in a primitive cell. (The element number of the primitive cell is 18,628 for $r/l = 0.43$). (For interpretation of the references to color in this figure, the reader is referred to the web version of this article.)

Young's moduli of the matrix of periodic cellular structures and the interfacial layers are E and E_0, respectively, and the Young modulus ratios $\alpha = E_0/E$ are in the range from 0.01 to 1,000,000, which covers most possibilities of materials composition, regardless of the interface layers are stronger or weaker than the matrix cellular structures. Poisson's ratio of the interfacial layers and the cellular matrix are assumed to be the same.

Numerical simulations are carried out using the commercial software ABAQUS, and neo-Hookean model is employed to model the material properties. All the RVE models of periodic cellular composites are meshed using the 6-node modified quadratic hybrid plane-strain triangle elements (ABAQUS element type CPE6MH). The element number varies as the radius-to-length ratios r/l changes and is about 20,000 in a unit cell of periodic cellular composites. Fig. 2(c) shows the mesh details of a unit cell with $r/l = 0.43$.

The instabilities of the RVE models are firstly investigated as an eigenvalue problem via the linear buckle analysis in ABAQUS. The linear buckling analysis will yield many eigenvalues and corresponding buckling modes, nevertheless, generally only the lowest eigenvalue with the corresponding buckling mode is of interest, because the buckling modes with higher eigenvalues are difficult to trigger under quasi-static loading conditions [44]. Therefore, the critical strain (corresponding to the first eigenvalue) can be estimated in the linear range of deformation. However, to obtain more accurate values of the critical strain, a post-buckling analysis must be performed. The first eigenmode is introduced as an initial geometric imperfection to the finite element model for the post-buckling analysis, and the analysis is conducted using ABAQUS/STANDARD including geometric nonlinearity.

2.1.2. Boundary conditions

In the RVE model, two reference points (R_x and R_y) are defined in order to implement the boundary condition. The uniaxial compression load is applied by giving a displacement c_y to R_y in y direction. The displacements of R_y in x direction and of R_x in y direction are set to zero, while the displacement of R_x in x direction is left free. To avoid the rigid motion of the model, the center of the left-bottom minimum unit is fixed by setting the displacement in the x direction to zero. With the coordinate system shown in Fig. 2(a), the periodic boundary condition is applied on the parallel opposite edges, which can be expressed as follows,

$$\begin{aligned} &u_x(L_x,y) - u_x(0,y) = \bar{\varepsilon}_x L_x = c_x \\ &u_y(L_x,y) - u_y(0,y) = 0 \\ &u_x(x,L_y) - u_x(x,0) = 0 \\ &u_y(x,L_y) - u_y(x,0) = \bar{\varepsilon}_y L_y = c_y \end{aligned} \tag{1}$$

where $u_i(x,y)$ means the displacement vector at coordinate (x,y), L_i and $\bar{\varepsilon}_i$ represents the length and average strain of the RVE model, respectively, and c_i represents the displacement of the reference point R_i in i direction, $i = x,y$.

2.2. Experimental studies

The single-material periodic cellular structures are fabricated by synthesizing PDMS (the elastomer base to cross-linker ratio is 30:1), and the sizes of samples are about 78 mm × 78 mm × 9.5 mm, the radii of the circular holes are measured to be $r = 3.18 \pm 0.03$ mm and $r = 3.45 \pm 0.03$ mm for two different samples, the nearest center-to-center spacing is measured to be $l = 9.75$ mm.

The periodic cellular composite structures are fabricated via two methods: one is by printing with a multi-material 3D printer (Object350 Connex3, Stratasys Inc., USA); and the other one is by synthesizing PDMS with different interfacial layers, such as PET film or steel slice.

Two polymers were used in the 3D printing: Vero White and Tango Black Plus. Vero White is a rigid plastic at room temperature with Young's modulus measured to be about 1.75 GPa, while Tango Black Plus is a rubbery material at room temperature with Young's modulus measured to be about 1.15 MPa. The matrix phase of periodic cellular structures was printed in Tango Black Plus, while the interfacial layers were printed in Vero White, which gives a Young's modulus ratio of about $\alpha = 1500$. The size of sample is 80 mm × 80 mm × 10 mm, and the thicknesses of interfacial layers are $t = 0.1$ mm.

As for the second method, an acrylic mold was first made with a laser cutting machine from a thick acrylic plate, as shown in Fig. 6(a). Then, the PET film or steel slice was spliced into a frame as the green lines showed in Fig. 2. Finally, the cellular composites were fabricated by synthesizing PDMS in the mold with the spliced frame in it. The elastomer base to cross-linker ratio of PDMS for the cellular composites with PET film and steel slice are 50:1 and 30:1, respectively. As shown in Fig. 6(b)–(c), the sizes of samples fabricated with the mold are 40 mm × 40 mm × 10 mm, the radii of circular holes are measured to be $r = 3.05$ mm, and the thicknesses of the interfacial layers are $t = 0.048$ mm (PET film) and $t = 0.049$ mm (steel slice), respectively.

Young's modulus of PDMS with different ratio of elastomer base to cross-linker for 30:1 and 50:1 are measured to be about 0.7 MPa and 0.05 MPa, respectively. Young's modulus for the steel slice is about 210 GPa and for PET film is about 2 GPa, thus the modulus ratio of the two samples are $\alpha = 300{,}000$ and $\alpha = 40{,}000$, respectively.

The uniaxial compression tests were performed using an "SHIMADZU AGS-X50N" machine with a 1 kN load cell, and the load rate is about 0.133 mm/s. Acrylic sheets were used to help eliminate the out-of-plane buckling.

3. Results and discussion

3.1. Buckling of composite periodic cellular structures with soft matrix and interfacial layers

The buckling patterns of periodic cellular composites with soft matrix and interfacial layers are investigated through numerical simulations and experimental studies, respectively. Based on the linear buckle analysis in ABAQUS, we summarize the wrinkling patterns of the RVE model with 2 × 2 primitive cells into a phase diagram as shown in Fig. 3.

From Fig. 3, it can be observed that the instability can be partitioned into four different modes, which are marked with different colors respectively: The red region (I) and the light blue region (II) both represent the global buckling mode as shown in Fig. 3(a) and (b), but the interfacial layers of the models in region II are buckled additionally as shown in Fig. 3(b); the blue region (III) represents the pure interfacial wrinkling mode as shown in Fig. 3(c); and the black region (IV) represents the local buckling mode as shown in Fig. 3(d). When it lies on the intersection lines between two regions, the buckling modes possesses both features of the two regions. For example, the buckling mode corresponding to the point ($\alpha = 2000$, $r/l = 0.32$) in the red circle which lies on the intersection between regions (III) and (IV), owns the features of both local buckling mode and the interfacial wrinkling mode as shown in Fig. 3(e); and buckling mode corresponding to the point ($\alpha =$ 200,000, $r/l = 0.33$) in the blue circle which lies on the intersection between regions (I) and (IV), has the characteristics of both global buckling mode and local buckling mode as shown in Fig. 3(f).

From the phase diagram in Fig. 3, we can draw the following interesting conclusions. First, when the Young's modulus ratio α is large enough, the periodic cellular composites will present the global buckling mode without additional buckling interfacial layers and are independent of the radius-to-length ratio r/l. Second, for the case $\alpha = 1$, since Poisson's ratios of the interfacial layers and the cellular matrix are assumed to be the same, the composite periodic cellular structure become a single-material periodic cellular structure, and the smallest radius-to-length ratio r/l for pattern transformation is about 0.27 corresponding to a porosity of 0.229, which is different from 0.34 provided by Bertoldi et al. [8]; The reason for the difference will be explained later. Third, though the regions (II) and (IV) are separated by the region (III) in the radius-to-length ratio range $0.24 \le r/l < 0.37$, the intersection between regions (II) and (IV) are in the same line for the whole range, thus the post-buckling for the composites in region (III) should also be separated into two modes (global buckling and local buckling) by the dash green line, in fact, the post-buckling analysis also proves this. Fourth, when the Young modulus ratio $\alpha < 0.1$, the bonding of the composite structures may be too weak to bear the compressive load, thus resulting to no buckling modes, as presented in Fig. 3 by the white region with hollow squares, and it is more obvious when the radius-to-length ratio r/l is smaller.

The critical strain for first eigenmode of pattern transformation (local buckling mode) converges to that of 2 m × 2 m (m = 1,2, …) primitive cells; but the critical stain for second eigenmode of global buckling monotonically decreases with increasing RVE sizes [55]. Thus, we can conclude that, with a smaller RVE size, the critical strain for global buckling is much higher than that of pattern transformation. On the other hand, as the porosity of periodic cellular structures decreases, the critical strain for pattern transformation increases more quickly than that of global buckling [8]. Thus, we can expect that the critical porosity, at which the critical strain for pattern transformation is no longer smaller than that of global buckling, will be lower with a smaller RVE size and the regions corresponding to global buckling modes will enlarge with a larger RVE size.

To validate this, we have performed simulations with RVE models consist of 4 × 4 primitive cells, and a similar phase diagram can be obtained as shown in Fig. 4. It can be observed that the instability can also be partitioned into four different modes, which are marked with different colors respectively. Both the weak region and the global buckling regions are larger, while the pattern transformation region is

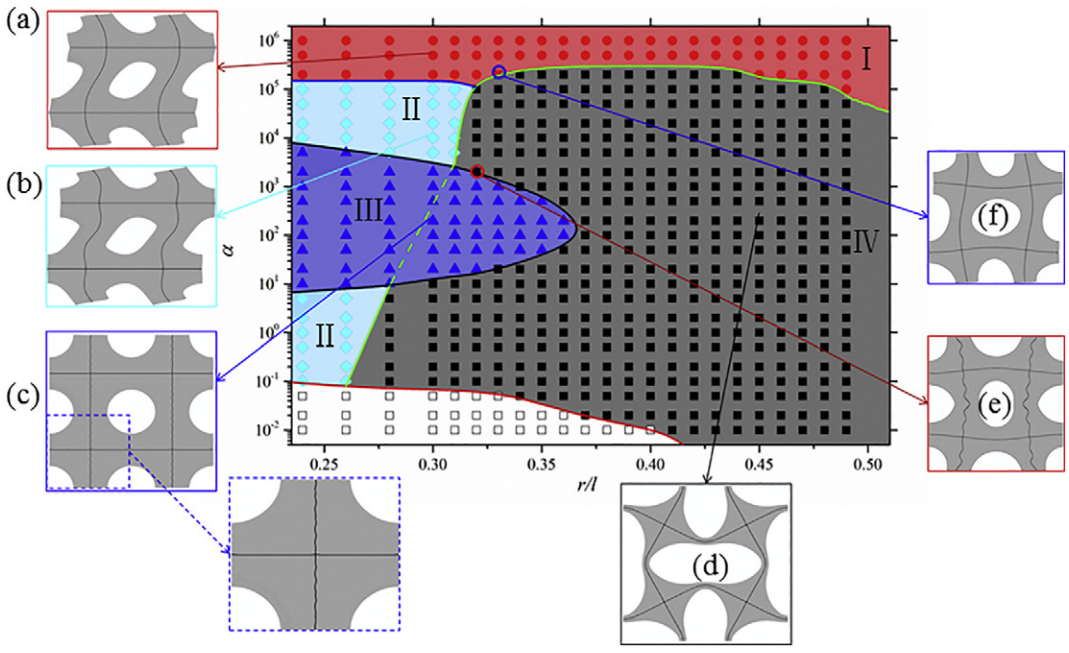

Fig. 3. Phase diagram of the buckling modes of composite periodic cellular structures with 2 × 2 primitive cells. The solid and hollow dots represent the composite periodic cellular structures with different Young's modulus ratio α and radius-to-length ratio r/l. There are four types of buckling modes, i.e., the global buckling pattern without additional buckling interfacial layers (I), the global buckling pattern with additional buckling interfacial layers (II), the pure interfacial wrinkling pattern (III), and the local buckling pattern (IV). The representative patterns corresponding to the four buckling modes are presented as figures (a)–(d), respectively. (e) represents the buckling mode of the intersection between (III) and (IV), which possesses both the features of these two modes. (f) represents the buckling mode of the intersection between (I) and (IV), which possesses the features of both global buckling and local buckling. The white region with hollow squares represent that the composite structures are not robust because of the weak interface layers. (For interpretation of the references to color in this figure, the reader is referred to the web version of this article.)

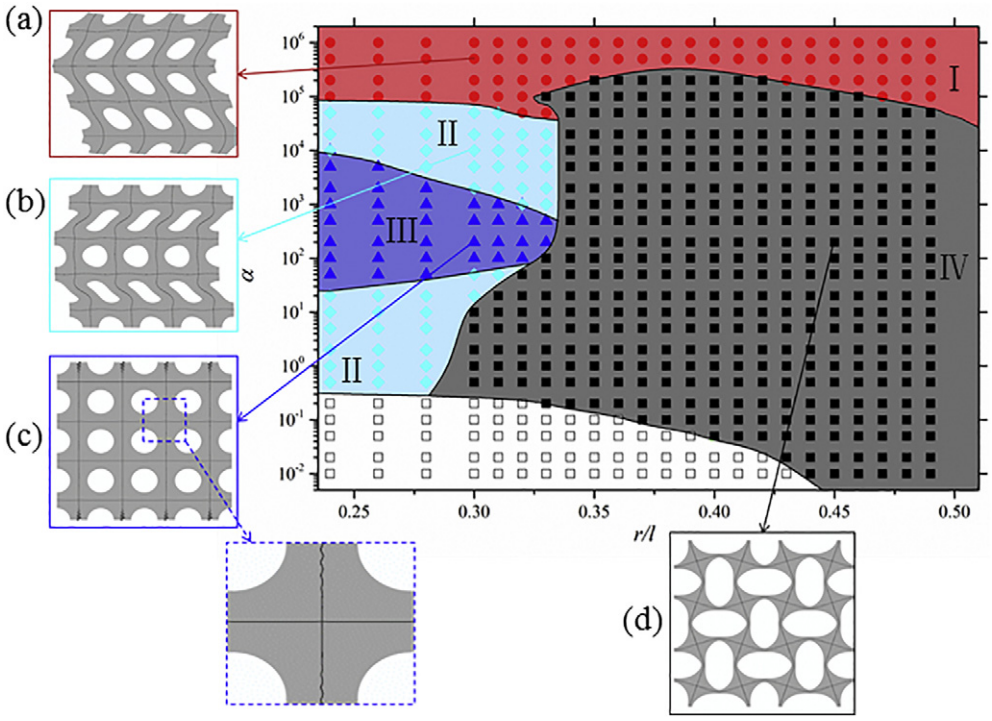

Fig. 4. Phase diagram of the buckling modes of composite periodic cellular structures with 4 × 4 primitive cells. The solid and hollow dots represent the composite periodic cellular structures with different Young's modulus ratio α and radius-to-length ratio r/l. There are four types of buckling modes, i.e., the global buckling pattern (I) and (II), the pure interfacial wrinkling pattern (III), and the local buckling pattern (IV). The representative patterns corresponding to the five buckling modes are presented as figures (a)–(d), respectively. The white region with hollow squares represent that the composite structures are not robust because of the weak interface layers.

smaller, in comparison with Fig. 3. From the case $\alpha = 1$, we can obtain the smallest radius-to-length ratio r/l for pattern transformation is about 0.29 corresponding to a porosity of 0.264, which is larger than the critical porosity obtained with the RVE models consist of 2 × 2 primitive cells. Therefore, the conclusion is that the porosity for pattern transformation is smaller with a RVE model of smaller size is proved to be right, and we can conclude that the RVE size should be larger than 4 × 4 primitive cells in Bertoldi et al. [8]. However, we focus on the critical strains for pattern transformation, which is independent of RVE size as long as the RVE model is consist of 2 m × 2 m (m = 1,2, …) primitive cells [55], so numerical simulations with RVE models consist of >4 × 4 primitive cells will not be included in this paper.

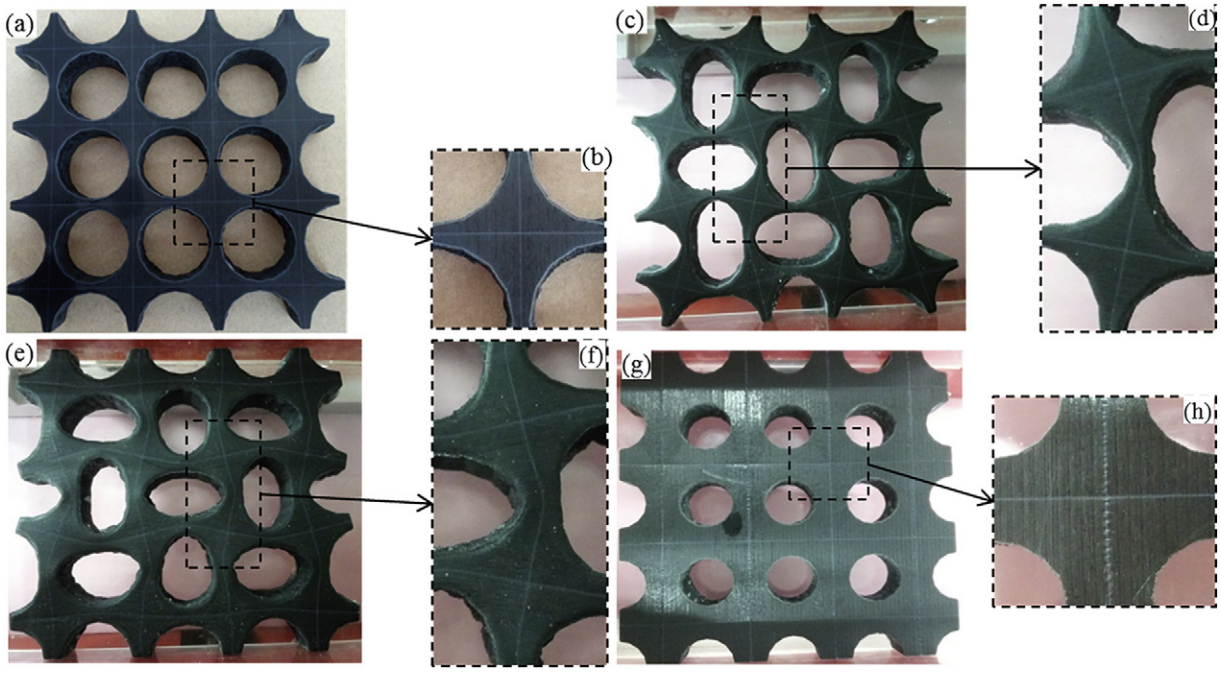

Fig. 5. Images of the cellular composites by 3D printing with different radius-to-length ratio r/l. (a)–(b): The initial shape of the sample with r/l = 0.45 ((a) the full sample, (b) the local image of the sample). (c)–(d): The buckling shape of the sample with r/l = 0.45 ((c) the full sample, (d) the local image of the sample). (e)–(f): The buckling shape of the sample with r/l = 0.4 ((e) the full sample, (f) the local image of the sample). (g)–(h): The buckling shape of the sample with r/l = 0.3 ((g) the full sample, (h) the local image of the sample).

With the 3D printing method, one of the samples with a radius-to-length ratio $r/l = 0.45$ is shown in Fig. 5(a), and the buckling pattern is shown in Fig. 5(c)–(d). Fig. 5(e)–(f) and (g)–(h) illustrate the buckling pattern of the samples with radius-to-length ratios $r/l = 0.4$ and $r/l = 0.3$, respectively. As for the second method, the initial and buckling patterns of the samples are presented in Fig. 6.

From the experimental images of buckling patterns shown in Figs. 5 and 6, we can see that, the buckling patterns of periodic cellular composites and interfacial layers agree well with the prediction as illustrated in Fig. 3. The different buckling patterns corresponding to the predicted distribution in Fig. 3 can be activated with suitable Young's modulus ratio α and porosity ϕ (or radius-to-length ratio r/l).

3.2. Characterization of the pattern transformation in single-material periodic cellular structures

Since pattern transformation is indeed a kind of elastic instability, the weakest section of the periodic cellular structure dominates the instability. To provide a theoretical prediction for the pattern transformation of periodic cellular structures, we make the following assumptions and simplifications. As shown in Fig. 7, the cellular structures with circular holes of radius r and center-to-center spacing l are first replaced by a structure with square holes, that is, a cross-shaped structure with a finite width $d = l - 2r$. Then, the cross-shaped structure with a finite width is simplified as a cross frame consisting of bars with rigid joints. Thus, we can apply Euler's column formula to study the pattern transformation. However, Euler's column formula is only applicable to slender bars, which means that the radii of the circular holes should be large enough; hence other formulas should be employed to characterize the buckling of periodic cellular structures with rather small radii.

However, the critical stress for local buckling mode of a square lattice is always higher than the stress needed to trigger the global buckling mode [41–43], hence a higher order buckling mode is employed in analyzing the pattern transformation of periodic cellular structures with circular holes. The cross frame in Fig. 7(c) is symmetrical with respect to horizontal and vertical axes, and each member of the framework with rigid joints can be treated as a bar with elastically restrained ends. The vertical members of the frames are compressed by an axial force F, and it is assumed that lateral movement of the joints is prevented by external constraints. When the load F reaches a critical value, the vertical bars begin to buckle as indicated by the green lines. This buckling is accompanied by the bending of horizontal bars, and these bars will exert reactive moments at the joints of vertical bars. Hence, the vertical bars can be treated as bars with elastically built-in ends [52].

Consider a simply supported horizontal bar subjected to two equal and opposite couples at each hinge joints, the bending moments are proportional to the rotation angle θ at the joints with the following relationship,

$$M_0 = \frac{2EI}{l}\theta \tag{2}$$

where EI and l denote the flexural rigidity and length of the bar, respectively.

The moment of vertical bar can be expressed by the following equilibrium differential equation

$$M(y) = EIy'' = -Fy + M_0 \tag{3}$$

where y and y'' are the deflection and the second order derivative of deflection of the vertical bar, respectively.

Substituting Eq. (2) into Eq. (3), we can obtain

$$y'' + k^2 y = \frac{2\theta}{l} \tag{4}$$

where $k^2 = F/(EI)$.

Eq. (4) is a second order linear non-homogeneous differential equation with constant coefficients, and the general solution is

$$y = A\ \sin kx + B\ \cos kx + \frac{2\theta}{k^2 l} \tag{5}$$

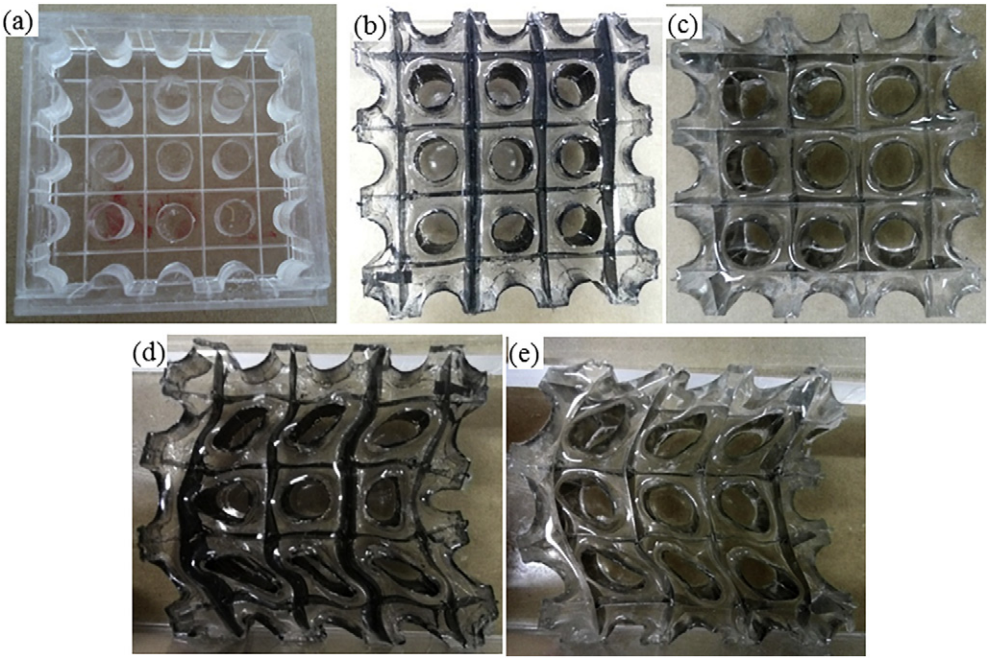

Fig. 6. (a) The acrylic mold for synthesizing cellular composite samples with PDMS. (b)–(e) Images of the cellular composites before ((b)–(c)) and after ((d)–(e)) buckling. The radius-to-length ratio is $r/l = 0.305$, and the PDMS for the cellular composites with PET film and steel slice are 50:1 and 30:1, respectively.

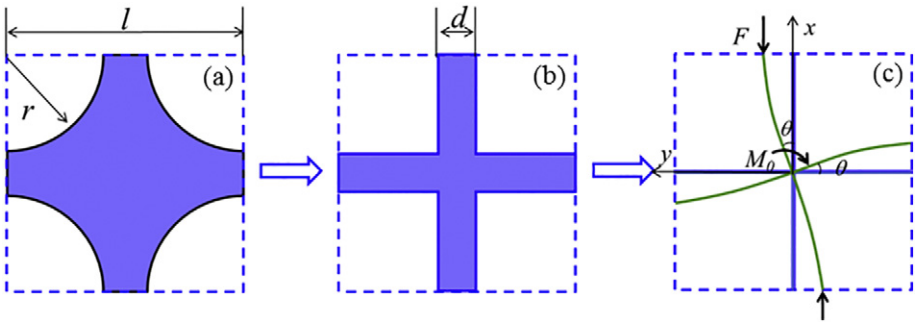

Fig. 7. Schematic of the simplification of periodic cellular structure into a cross frame. (a) The initial periodic cellular structures with circular holes (radius r and center-to-center spacing l). (b) The cross-shape structure with a finite width ($d = l - 2r$) after first simplification. (c) The cross frame structure after second simplification and the green lines indicate the buckling geometry when the load F reaches its critical value. (For interpretation of the references to color in this figure legend, the reader is referred to the web version of this article.)

Consider the following boundary conditions

$$\begin{cases} y(0) = B + \dfrac{2\theta}{k^2 l} = 0 \\ y'(0) = Ak = \theta \\ y'(l/2) = Ak\cos\dfrac{kl}{2} - Bk\sin\dfrac{kl}{2} = 0 \end{cases} \tag{6}$$

We can obtain

$$\tan\frac{kl}{2} + \frac{kl}{2} = 0 \tag{7}$$

which gives $kl \approx 4.058$, hence the critical force corresponding to the buckling of the frame can be deduced as

$$F_{cr} = k^2 EI = \frac{16.47EI}{l^2} \tag{8}$$

According to the general form of Euler's column formula, Eq. (8) can be expressed as follows,

$$F_{cr} = \frac{\pi^2 EI}{(\mu l)^2} \tag{9}$$

where μl is the reduced length of the compressed bar and $\mu = 0.774$.

Let $i = \sqrt{I/A}$ represents the radius of gyration and $I = (l-2r)^3/12$ is the moment of inertia; the critical stress can be derived as

$$\sigma_{cr} = \frac{F_{cr}}{A} = \frac{\pi^2 E}{(\mu l/i)^2} = \frac{\pi^2 E}{\lambda^2} \tag{10}$$

where $A = l - 2r$ and $\lambda = \mu l/i$ are the cross-sectional area and slenderness ratio of the bar, respectively. The critical stress depends only on the slenderness ratio λ and Young's modulus E of the material.

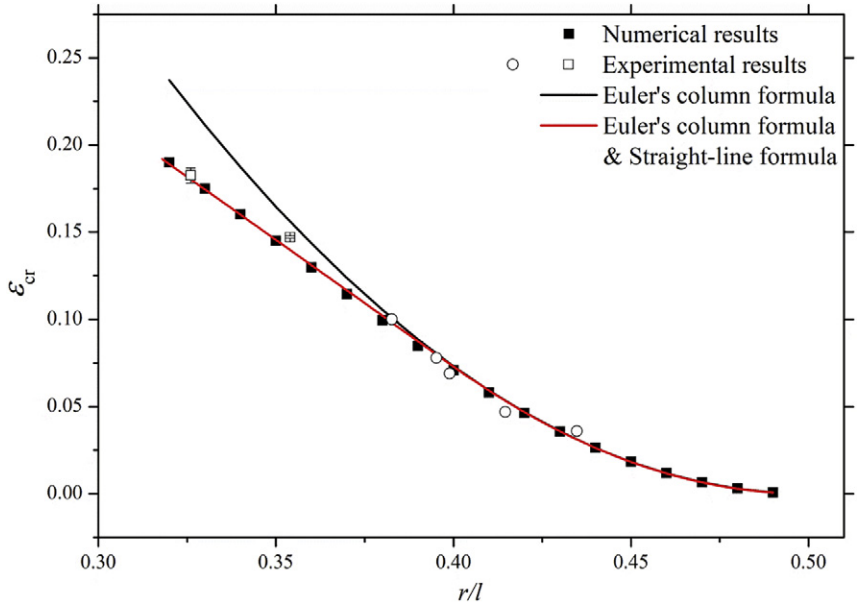

Fig. 8. Critical strains of periodic cellular structures with different value of r/l. The solid dots denote numerical results, the black line and red line represent the theoretical results by Euler's column formula without and with straight-line formula. The hollow circles represent the experimental results collected from previous studies [8,30,55,56], and the hollow squares represent our complementary experimental results. (For interpretation of the references to color in this figure legend, the reader is referred to the web version of this article.)

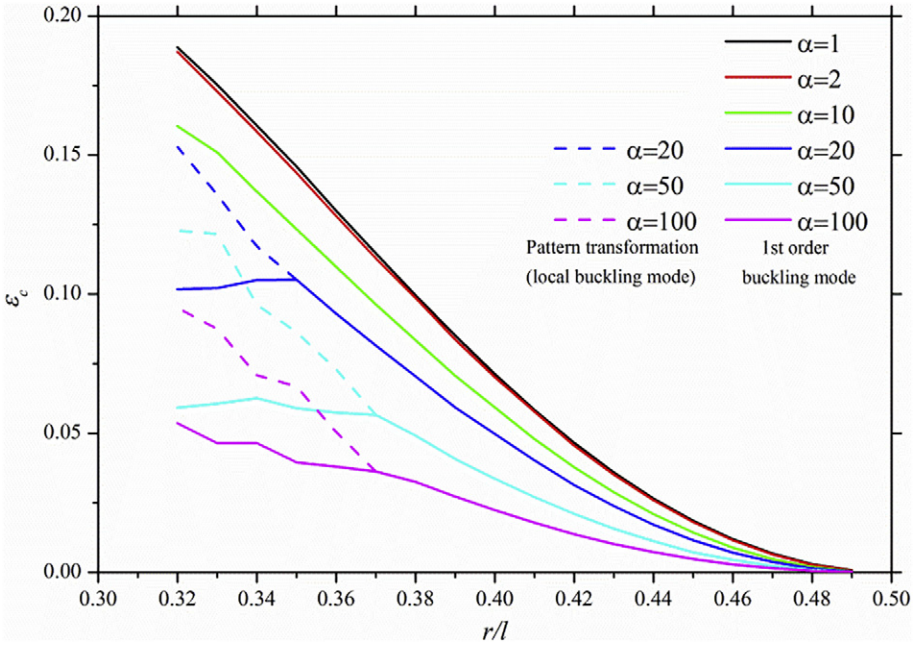

Fig. 9. Critical strains for the periodic cellular composites with interfacial layers of different Young's modulus ratio α and radius-to-length ratio r/l. The solid lines represent the critical strains for first-order buckling modes, and the dash lines represent the critical strains for pattern transformations (local buckling modes) when pattern transformation is not the first-order buckling mode.

Consider plane-strain problem, the critical stress in Eq. (10) can be rewritten as

$$\sigma_{cr} = \frac{\pi^2 E}{\lambda^2(1-\nu^2)} \tag{11}$$

where ν is Poisson's ratio of the material.

Thus, the critical value of nominal strain corresponding to the buckling can be deduced as

$$\varepsilon_{cr} = \frac{\sigma_{cr}}{E} = \frac{\pi^2}{\lambda^2(1-\nu^2)} \tag{12}$$

From Eq. (12), it can be found that the critical strain only depends on the slenderness ratio λ and Poisson's ratio ν of the material, and is independent of the material's Young's modulus E, which is consistent with the well-known property of metamaterials that the equivalent physical properties of metamaterials are governed by their architectures rather than compositions. The effect of Poisson's ratio is introduced due to the plane-strain assumption.

However, since the above discussions assume that the bar is very slender, i.e. the expression is only valid for bars with high slenderness ratios. For bars with low slenderness ratios, empirical formulas, such as straight-line formula and parabolic formula, should be employed.

To validate the scope of application of formula (12) for a 2D problem, we carry out finite element simulations with different RVE models, and the critical strains for each model are presented as square dots in Fig. 8. The finite element simulation results agree well with the theoretical prediction of (12) derived from Euler's column formula when $r/l > 0.405$ (i.e., $\phi > 0.515$) and depart from that prediction to an approximately linear behavior when $r/l \le 0.405$. The linear behavior can be represented by a straight-line formula $\varepsilon_{cr} = 0.653 - 1.45r/l$ by fitting the simulation results. Thus, the critical strains of periodic cellular structures with different value of r/l can be predicted as

$$\varepsilon_{cr} = \begin{cases} \dfrac{\pi^2}{\lambda^2(1-\nu^2)}, & \dfrac{r}{l} > 0.405 \\ 0.653 - 1.45\dfrac{r}{l}, & \dfrac{r}{l} \le 0.405 \end{cases} \tag{13}$$

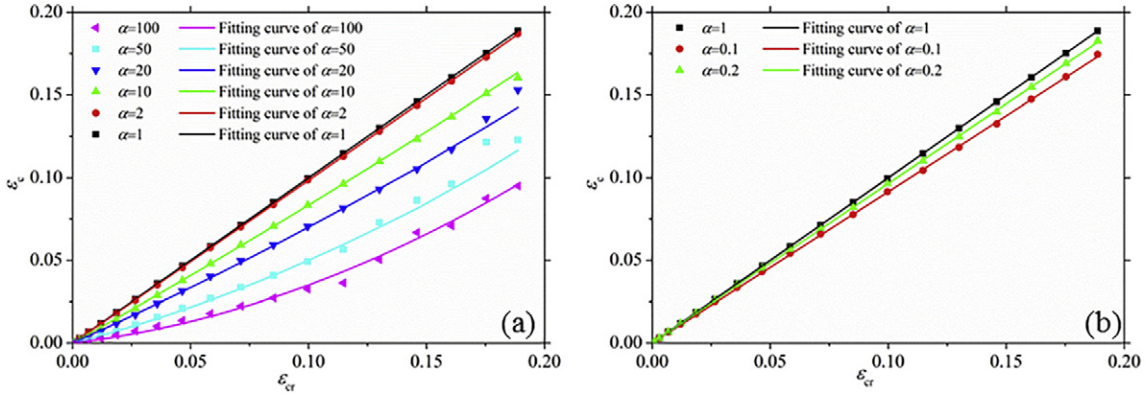

Fig. 10. Critical strains for different Young's modulus ratios ((a)$\alpha > 1$ and (b) $\alpha < 1$) in relation to the critical strains for $\alpha = 1$ (single-material periodic cellular structures). The dots represent numerical results, and the solid lines represent the fitting curves for the numerical results.

Table 1
Values of β_1 and β_2 for different Young's modulus ratios α.

α	0.1	0.2	1	2	10	20	50	100
β_1	0.91173	0.96623	1	0.97858	0.798	0.64338	0.36975	0.17249
β_2	0.03001	0.01294	0	0.05563	0.36512	0.59482	1.31541	1.77847

The hollow circles in Fig. 8 are the experimental results collected from previous studies [8,30,55,56]. However, the existing experimental results in previous reports are only for larger porosities. Therefore, we performed two complementary experiments with radius-to-length ratios about $r/l = 0.354$ and 0.326, and the complementary experimental results are shown as the hollow squares in Fig. 8. The experimental results also validate the prediction of formula (13).

3.3. Characterization of the pattern transformation in composite periodic cellular structures

The local buckling modes correspond to the pattern transformation of periodic cellular composites with interfacial layers. Consider cases in the range of $0.32 \le r/l \le 0.49$ and $1 \le \alpha \le 100$, with appropriate initial geometric imperfections corresponding to different eigenmodes (first-order buckling mode or local buckling mode) introduced to the finite element model, the critical strains for each case can be obtained through the post-buckling analysis in the finite element simulation are shown in Fig. 9. As we can see from Fig. 3, the first buckling modes of the periodic cellular composites are pattern transformation unless $\alpha \ge 20$ and $r/l \le 0.37$. The critical strains for the first-order buckling of periodic cellular composites are presented in solid lines as shown in Fig. 9. If the first-order buckling is not pattern transformation, the local buckling mode is introduced as the initial geometric imperfection to trigger the pattern transformation during the post-buckling analysis and the critical strain for that kind of pattern transformation is depicted in dash lines shown in Fig. 9.

From Fig. 9, we can observe that, if the Young's modulus ratio α is constant, the critical strains and the radius-to-length ratios have one-to-one corresponding relations, hence we could utilize the critical strains ε_{cr} for $\alpha = 1$ (which are also the critical strains for corresponding single-material periodic cellular structure with the same porosities) to represent the radius-to-length ratios r/l. Accordingly, the critical strains ε_c for other Young's modulus ratios in Fig. 9 can be re-plotted in relation to ε_{cr} in dots shown in Fig. 10(a). Similarly, we could obtain the relationships between the critical strains for $\alpha < 1$ and $\alpha = 1$, which are plotted in dots shown in Fig. 10(b).

From the results in Fig. 10, we can draw the following conclusions: First, just by introducing very thin interfacial layers into the periodic cellular structures, the critical strain for pattern transformation can be significantly influenced. Second, regardless of the interfacial layer is harder ($\alpha > 1$) or softer ($\alpha < 1$) than the matrix periodic cellular structure, the critical strains for composite periodic cellular structures are all lower than the single-material periodic structures. This is because the critical buckling strains for the interfacial layers is very small because of their thin sections, thus the buckling of the interfacial layers will introduce imperfections to the periodic cellular composites and trigger the composites buckling. Third, the larger the difference between the Young modulus of the interfacial layers and the matrix materials, the more significant the critical strain drops.

Besides, we found that the relationship between the critical strains for $\alpha = 1$ and other Young's modulus ratios follow formulas in a same form, which can be expressed as follows

$$\varepsilon_c = \beta_1 \varepsilon_{cr} + \beta_2 \varepsilon_{cr}^2 \tag{14}$$

where ε_{cr} and ε_c represent the critical strains for $\alpha = 1$ (single-material periodic cellular structure) and other Young's modulus ratios (composite periodic cellular structures), respectively. The values of the parameters β_1 and β_2 are fitted and listed in Table 1.

Furthermore, the values of β_1 and β_2 follow respective the algebra expressions in relation to α as shown in Fig. 11 and the relationships can be expressed as follows,

$$\begin{aligned} \beta_1 &= 1 - 0.067 \cdot \lg\alpha - 0.17 \cdot (\lg\alpha)^2 \\ \beta_2 &= 0.065 \cdot \lg\alpha + 0.19 \cdot (\lg\alpha)^2 + 0.11 \cdot (\lg\alpha)^3 \end{aligned} \tag{15}$$

As we can see from Eqs. (14)–(15), the critical strains ε_c for periodic cellular composites only depend on the Young's modulus ratio α and the critical strain ε_{cr} for the corresponding single-material periodic cellular structure with a same radius-to-length ratio r/l. The critical strain ε_{cr} for the corresponding single-material periodic cellular structure can be attained from Eq. (13), once the radius-to-length ratio r/l and Poisson's ratio ν are known. Thus, for the type of periodic cellular composites with a thickness-to-length ratio $t/l = 0.005$ in this study, the

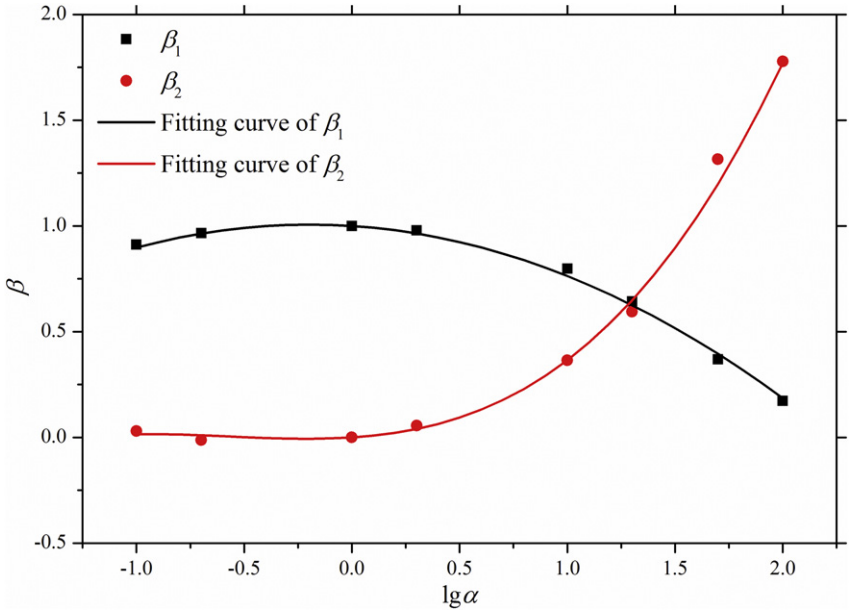

Fig. 11. The curves of β_1 and β_2 as a function of Young's modulus ratio α.

critical strain for pattern transformation can be predicted by Eq. (13)–(15), when the periodic cellular composites with different α and r/l are compressed.

4. Conclusions

In this study, a new composite periodic cellular structure with interfacial layers is developed and its buckling modes are explored through experimental studies and numerical simulations. When the periodic cellular composites are applied with a uniaxial compression loading and compressed beyond a critical value, many interesting novel phenomena can be found. The most exciting thing is that, just by introducing very thin interfacial layers into the periodic cellular structures, the critical strain for pattern transformation can be significantly influenced and is always lower than the single-material periodic cellular structure, regardless of the interfacial layer is stiffer or softer than the matrix materials. Besides, we proposed a theoretical method to predict the critical strain for pattern transformation of single-material periodic cellular structures, and the theoretical prediction agrees quite well with the experiment and simulation results. Finally, based on the simulation and experimental results of composite periodic cellular structures, the theoretical method is further developed to predict the critical strain for a definite range of combinations of the materials and porosities of the periodic cellular composites. The study provides a promising development of architected metamaterials and offers the possibility to control the buckling critical strain of periodic cellular structures, thus may widen the applications of this kind of structures.

Acknowledgements

The authors are grateful for the support from the National Natural Science Foundation of China through grant numbers 11321062, 11372236 and 11572236.

References

[1] J.-H. Lee, J.P. Singer, E.L. Thomas, Micro-/nanostructured mechanical metamaterials, Adv. Mater. 24 (36) (2012) 4782–4810.
[2] C. Coulais, E. Teomy, K. de Reus, Y. Shokef, M. van Hecke, Combinatorial design of textured mechanical metamaterials, Nature 535 (7613) (2016) 529–532.
[3] B.A. Slovick, Negative refractive index induced by percolation in disordered metamaterials, Phys. Rev. B 95 (9) (2017), 094202.
[4] D.R. Smith, J.B. Pendry, M.C.K. Wiltshire, Metamaterials and negative refractive index, Science 305 (5685) (2004) 788–792.
[5] Z. Li, M. Mutlu, E. Ozbay, Chiral metamaterials: from optical activity and negative refractive index to asymmetric transmission, J. Opt. 15 (2) (2013), 023001.
[6] J. Valentine, S. Zhang, T. Zentgraf, E. Ulin-Avila, D.A. Genov, G. Bartal, X. Zhang, Three-dimensional optical metamaterial with a negative refractive index, Nature 455 (7211) (2008) 376–379.
[7] S. Babaee, J. Shim, J.C. Weaver, E.R. Chen, N. Patel, K. Bertoldi, 3d soft metamaterials with negative Poisson's ratio, Adv. Mater. 25 (36) (2013) 5044–5049.
[8] K. Bertoldi, P.M. Reis, S. Willshaw, T. Mullin, Negative Poisson's ratio behavior induced by an elastic instability, Adv. Mater. 22 (3) (2010) 361–366.
[9] N.G. Joseph, C.-G. Roberto, R.D. Mirosław, W.W. Krzysztof, G. Ruben, Smart metamaterials with tunable auxetic and other properties, Smart Mater. Struct. 22 (8) (2013), 084016.
[10] X. Ren, J. Shen, A. Ghaedizadeh, H. Tian, Y.M. Xie, Experiments and parametric studies on 3d metallic auxetic metamaterials with tuneable mechanical properties, Smart Mater. Struct. 24 (9) (2015), 095016.
[11] X. Ren, J. Shen, A. Ghaedizadeh, H. Tian, Y.M. Xie, A simple auxetic tubular structure with tuneable mechanical properties, Smart Mater. Struct. 25 (6) (2016), 065012.
[12] K. Wang, Y.-H. Chang, Y. Chen, C. Zhang, B. Wang, Designable dual-material auxetic metamaterials using three-dimensional printing, Mater. Des. 67 (2015) 159–164.
[13] H. Chen, C.T. Chan, Acoustic cloaking in three dimensions using acoustic metamaterials, Appl. Phys. Lett. 91 (18) (2007) 183518.
[14] Z. Jian, C. Tianning, L. Qingxuan, W. Xiaopeng, X. Jie, J. Ping, A unidirectional acoustic cloak for multilayered background media with homogeneous metamaterials, J. Phys. D. Appl. Phys. 48 (30) (2015) 305502.
[15] H.M. Kolken, A. Zadpoor, Auxetic mechanical metamaterials, RSC Adv. 7 (9) (2017) 5111–5129.
[16] F. Song, J. Zhou, X. Xu, Y. Xu, Y. Bai, Effect of a negative Poisson ratio in the tension of ceramics, Phys. Rev. Lett. 100 (24) (2008) 245502.
[17] R. Lakes, Foam structures with a negative Poisson's ratio, Science 235 (4792) (1987) 1038–1040.
[18] F. Steffens, S. Rana, R. Fangueiro, Development of novel auxetic textile structures using high performance fibres, Mater. Des. 106 (2016) 81–89.
[19] M. Schenk, S.D. Guest, Geometry of miura-folded metamaterials, Proc. Natl. Acad. Sci. 110 (9) (2013) 3276–3281.
[20] Y. Tang, J. Yin, Design of cut unit geometry in hierarchical kirigami-based auxetic metamaterials for high stretchability and compressibility, Extreme Mech. Lett. 12 (2017) 77–85.
[21] S. Shan, S.H. Kang, Z. Zhao, L. Fang, K. Bertoldi, Design of planar isotropic negative Poisson's ratio structures, Extreme Mech. Lett. 4 (2015) 96–102.
[22] J.N. Grima, K.E. Evans, Auxetic behavior from rotating squares, J. Mater. Sci. Lett. 19 (17) (2000) 1563–1565.
[23] C.S. Ha, M.E. Plesha, R.S. Lakes, Chiral three-dimensional lattices with tunable Poisson's ratio, Smart Mater. Struct. 25 (5) (2016), 054005.
[24] D. Mousanezhad, B. Haghpanah, R. Ghosh, A.M. Hamouda, H. Nayeb-Hashemi, A. Vaziri, Elastic properties of chiral, anti-chiral, and hierarchical honeycombs: a simple energy-based approach, Theor. Appl. Mech. Lett. 6 (2) (2016) 81–96.
[25] F. Javid, E. Smith-Roberge, M.C. Innes, A. Shanian, J.C. Weaver, K. Bertoldi, Dimpled elastic sheets: a new class of non-porous negative Poisson's ratio materials, Sci Rep 5 (2015) 18373.
[26] H. Tan, L. Yu, Z. Zhou, Negative Poisson's ratio in non-porous smooth curve sheet, Physica Status Solidi (b), 2017 (1600612–n/a).
[27] D. Rayneau-Kirkhope, C. Zhang, L. Theran, M.A. Dias, Analytic analysis of auxetic metamaterials through analogy with rigid link systems, arXiv Preprint arXiv: 1703.05150, 2017.
[28] J. Liu, T. Gu, S. Shan, S.H. Kang, J.C. Weaver, K. Bertoldi, Harnessing buckling to design architected materials that exhibit effective negative swelling, Adv. Mater. 28 (31) (2016) 6619–6624.
[29] Z.S. Liu, W. Toh, T.Y. Ng, Advances in mechanics of soft materials: a review of large deformation behavior of hydrogels, Int. J. Appl. Mech. 7 (05) (2015) 1530001.
[30] T. Mullin, S. Deschanel, K. Bertoldi, M.C. Boyce, Pattern transformation triggered by deformation, Phys. Rev. Lett. 99 (8) (2007), 084301.
[31] K. Bertoldi, M.C. Boyce, Mechanically triggered transformations of phononic band gaps in periodic elastomeric structures, Phys. Rev. B 77 (5) (2008), 052105.
[32] Y. Chen, F. Scarpa, C. Remillat, I. Farrow, Y. Liu, J. Leng, Curved Kirigami silicomb cellular structures with zero Poisson's ratio for large deformations and morphing, J. Intell. Mater. Syst. Struct. 25 (6) (2014) 731–743.
[33] K.-L. Chen, Y.-P. Cao, M.-G. Zhang, X.-Q. Feng, Indentation-triggered pattern transformation in hyperelastic soft cellular solids, CR Mec. 342 (5) (2014) 292–298.
[34] J.Y. Hu, Y.H. He, J.C. Lei, Z.S. Liu, Novel mechanical behavior of periodic structure with the pattern transformation, Theor. Appl. Mech. Lett. 3 (5) (2013), 054007.
[35] J.Y. Hu, Y.H. He, J.C. Lei, Z.S. Liu, S. Swaddiwudhipong, Mechanical behavior of composite gel periodic structures with the pattern transformation, Struct. Eng. Mech. 50 (5) (2014) 605–616.
[36] Y.H. He, S.S. Guo, Z.S. Liu, K.M. Liew, Pattern transformation of thermo-responsive shape memory polymer periodic cellular structures, Int. J. Solids Struct. 71 (2015) 194–205.
[37] D.W. Abueidda, M. Bakir, R.K. Abu Al-Rub, J.S. Bergström, N.A. Sobh, I. Jasiuk, Mechanical properties of 3D printed polymeric cellular materials with triply periodic minimal surface architectures, Mater. Des. 122 (2017) 255–267.
[38] S. Yuan, F. Shen, J. Bai, C.K. Chua, J. Wei, K. Zhou, 3D soft auxetic lattice structures fabricated by selective laser sintering: Tpu powder evaluation and process optimization, Mater. Des. 120 (2017) 317–327.
[39] V.V. Vasiliev, V.A. Barynin, A.F. Rasin, Anisogrid lattice structures – survey of development and application, Compos. Struct. 54 (2–3) (2001) 361–370.
[40] G.W. Kooistra, H.N. Wadley, Lattice truss structures from expanded metal sheet, Mater. Des. 28 (2) (2007) 507–514.
[41] B. Haghpanah, J. Papadopoulos, D. Mousanezhad, H. Nayeb-Hashemi, A. Vaziri, Buckling of regular, chiral and hierarchical honeycombs under a general macroscopic stress state, Proc. R. Soc. A Math. Phys. Eng. Sci. 470 (2167) (2014).
[42] N. Ohno, D. Okumura, T. Niikawa, Long-wave buckling of elastic square honeycombs subject to in-plane biaxial compression, Int. J. Mech. Sci. 46 (11) (2004) 1697–1713.
[43] D.J. Rayneau-Kirkhope, M.A. Dias, Recipes for selecting failure modes in 2-d lattices, Extreme Mech. Lett. 9 (2016) 11–20.
[44] A. Ghaedizadeh, J. Shen, X. Ren, Y. Xie, Tuning the performance of metallic auxetic metamaterials by using buckling and plasticity, Dent. Mater. 9 (1) (2016) 54.
[45] J. Shim, P. Wang, K. Bertoldi, Harnessing instability-induced pattern transformation to design tunable phononic crystals, Int. J. Solids Struct. 58 (2015) 52–61.
[46] K. Carolin, L.-R. Yvonne, A systematic approach to identify cellular auxetic materials, Smart Mater. Struct. 24 (2) (2015), 025013.
[47] Z. Ding, Z. Liu, J. Hu, S. Swaddiwudhipong, Z. Yang, Inhomogeneous large deformation study of temperature-sensitive hydrogel, Int. J. Solids Struct. 50 (16) (2013) 2610–2619.
[48] W. Hong, Z. Liu, Z. Suo, Inhomogeneous swelling of a gel in equilibrium with a solvent and mechanical load, Int. J. Solids Struct. 46 (17) (2009) 3282–3289.
[49] Z.S. Liu, S. Swaddiwudhipong, W. Hong, Pattern formation in plants via instability theory of hydrogels, Soft Matter 9 (2) (2013) 577–587.
[50] Y. Chen, T. Li, F. Scarpa, L. Wang, Lattice metamaterials with mechanically tunable Poisson's ratio for vibration control, Phys. Rev. Appl. 7 (2) (2017), 024012.
[51] H. Fan, F. Jin, D. Fang, Uniaxial local buckling strength of periodic lattice composites, Mater. Des. 30 (10) (2009) 4136–4145.
[52] S.P. Timoshenko, J.M. Gere, Theory of Elastic Stability, Second edition McGraw-Hill International Book Company, 1963.
[53] S. Heitkam, W. Drenckhan, D. Weaire, J. Fröhlich, Beam model for the elastic properties of material with spherical voids, Arch. Appl. Mech. 86 (1) (2016) 165–176.
[54] Y. Li, N. Kaynia, S. Rudykh, M.C. Boyce, Wrinkling of interfacial layers in stratified composites, Adv. Eng. Mater. 15 (10) (2013) 921–926.
[55] K. Bertoldi, M.C. Boyce, S. Deschanel, S.M. Prange, T. Mullin, Mechanics of deformation-triggered pattern transformations and superelastic behavior in periodic elastomeric structures, J. Mech. Phys. Solids 56 (8) (2008) 2642–2668.
[56] J.T.B. Overvelde, S. Shan, K. Bertoldi, Compaction through buckling in 2d periodic, soft and porous structures: effect of pore shape, Adv. Mater. 24 (17) (2012) 2337–2342.